

Fundamental Limits of Feedback Cooling Ultracold Atomic Gases

Zain Mehdi,^{1,*} Simon A. Haine,¹ Joseph J. Hope,¹ and Stuart S. Szigeti¹

¹*Department of Quantum Science and Technology and Department of Fundamental and Theoretical Physics, Research School of Physics, Australian National University, Canberra 2600, Australia*

(Dated: June 19, 2023)

We investigate the fundamental viability of cooling ultracold atomic gases with quantum feedback control. Our study shows that the trade-off between the resolution and destructiveness of optical imaging techniques imposes constraints on the efficacy of feedback cooling, and that rapid rethermalization is necessary for cooling thermal gases. We construct a simple model to determine the limits to feedback cooling set by the visibility of density fluctuations, measurement-induced heating, and three-body atomic recombination. We demonstrate that feedback control can rapidly cool high-temperature thermal clouds in quasi-2D geometries to degenerate temperatures with minimal atom loss compared to traditional evaporation. Our analysis confirms the feasibility of feedback cooling ultracold atomic gases, providing a pathway to new regimes of cooling not achievable with current approaches.

The efficient cooling of quantum systems is a critical aspect of modern quantum science applications [1–4], including for precision measurement [3, 5], quantum simulation [6, 7], and quantum information [8, 9]. A powerful tool for achieving this is feedback cooling, where the system is monitored and controlled in real-time [10]. Although feedback cooling has been demonstrated for trapped ion systems [11] and a wide range of quantum mechanical oscillators [12–20], its applicability to more complex, multi-mode systems, such as quantum gases, is still an open question. In the next few years, rapid advances in the feedback control of ultracold atomic gases are expected, thanks to recent technological advances in highly-configurable optical potentials [21–23]. This presents an exciting opportunity to explore the potential of feedback cooling for ultracold atomic gases, and to address the challenges and open questions related to this technique.

The potential benefits of feedback cooling ultracold atomic gases are significant. It may alleviate existing limits to achievable atom number ($\sim 10^7$ per shot) inherent to evaporative cooling techniques [24], or improve current limits to achievable degeneracy for given total atom number. This latter aspect may play a critical role in space-based quantum sensing applications, where thermal expansion of the atomic cloud is a limiting factor in achievable sensitivity [25]. Moreover, limits to achievable degeneracy are even more pronounced for Fermi gases, with state-of-the-art demonstrations falling at least an order of magnitude short of the required degeneracy needed to use Fermi gases as quantum simulators of high-temperature superconductivity [26].

However, a feedback-cooled ultracold atomic gas has not yet been experimentally realized, and furthermore it is unclear whether feedback cooling’s efficacy is sufficient to achieve the above benefits. Although there have been a number of theoretical investigations of feedback cooling in Bose gas systems [27–36], the methods employed in these studies are computationally intensive, contextually

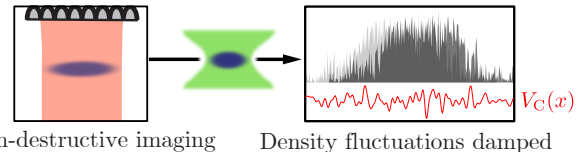


FIG. 1. Schematic of the feedback loop. The atomic cloud density (dark blue) is non-destructively imaged by an off-resonant optical field (red). Atomic density fluctuations (1D projection shown in grey) are then damped by a control potential V_C (red trace) which can be realized, for example, by a configurable optical-dipole potential (green).

bound, and usually limited to low-temperature gases in quasi-one-dimensional geometries, precluding their ability to study the viability of feedback cooling in general. Furthermore, there have been no studies of feedback cooling ultracold Fermi gases to date, and as such the effect of quantum statistics on the feedback scheme is poorly understood.

In this work, we assess the viability of feedback cooling ultracold gases by establishing fundamental limits imposed by the physics of non-destructive optical imaging and the thermodynamics of thermal cold-atom ensembles. We demonstrate the necessity of rapid rethermalization due to the constraints imposed by signal resolution and destruction due to measurement, concretely ruling out the possibility of feedback cooling single-component Fermi gases or one-dimensional integrable systems. We develop a continuous feedback cooling model for thermal gases, including multi-component systems, and use this to show that large atom number ($N \sim 10^9$), highly-oblate atomic gases can be feedback cooled to degeneracy with minimal atom loss. Our results establish feedback as a promising number-conserving approach to cooling ultracold gases in reduced dimensions and establishes a foundation for future investigations of feedback cooling single component Bose gases, as well as Bose-Fermi mixtures.

Feedback cooling scheme.— We consider a realistic

feedback cooling scheme (Fig. 1) based on models developed and validated in Refs. [29, 30, 32, 37], in which an atomic cloud is dispersively imaged by off-resonant coherent light illuminated along the tightly-trapped z -axis. The imaging gives a real-time estimate of the atomic column density in the xy plane, which is then used to construct a control potential that damps observable density fluctuations. This control can be applied using a configurable optical dipole potential [22], for example. For simplicity, we consider a cylindrically symmetric geometry $\omega_x = \omega_y \equiv \omega_{\perp}$ with $\kappa \equiv \omega_z/\omega_{\perp} \gg 1$ and assume the atomic density is well-described by a Gaussian of radial and transverse standard deviations R_{\perp}, R_z , respectively.

Direct control of thermal excitations.— In the absence of rethermalization, thermal excitations must be directly controlled, which is only possible if they are resolvable in the density image. Consequently, a parameter range for effective feedback cooling is given by fundamental bounds on the measurement resolution.

Firstly, the smallest possible lengthscale resolvable by optical imaging, Δr , is given by the geometric mean of the gas ‘thickness’ and light wavelength λ [29, 38]:

$$\Delta r^2 \leq \frac{R_z \lambda}{2\pi} \equiv r_D^2. \quad (1)$$

This resolution limit arises due to the fact that light rays cannot remain exactly parallel and diffract by a minimum angle as they pass through a sample of thickness R_z . A second limit is set by the measurement strength, which must be sufficiently strong to ensure an accurate estimate of the atomic density, yet sufficiently weak to avoid destruction of the atomic cloud via induced spontaneous emission. The signal-to-noise ratio (SNR) of a single pixel of area A from any non-destructive optical measurement of the atomic density with classical light is bounded by the shot-noise limit [39, 40]:

$$\text{SNR} \leq \frac{\tilde{n}}{2} \sqrt{\eta A \sigma_0 \Gamma P_e \delta t}, \quad (2)$$

where $\eta \in (0, 1]$ is the detector’s quantum efficiency, $\sigma_0 = 3\lambda^2/(2\pi)$ is the resonant optical cross section, \tilde{n} is the average column-density of the pixel, Γ is the excited state linewidth, P_e is the excited state probability, and δt is the integration time of the detector. The destruction associated with each measurement is quantified by the average number of spontaneous emission events per atom: $D \equiv \Gamma P_e \delta t$.

Useful feedback control requires $\text{SNR} \geq 1$. By considering a perfect ($\eta = 1$) measurement of the atomic cloud with the minimum $\text{SNR} = 1$ at a pixel with peak column density ($\bar{n} \leq \bar{n}_{\max} = N/(2\pi R_{\perp}^2)$ for a Gaussian density), we can derive a lower bound on the amount of acceptable destruction. A conservative estimate of the bound $\text{SNR} \geq 1$ is given by taking the zero-temperature limits for the radii of ideal Fermi and Bose gases –

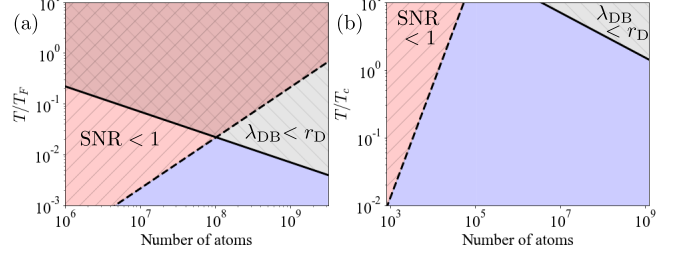


FIG. 2. Regions where thermal excitations are resolvable for degenerate Fermi (a) and Bose (b) gases. The solid and dashed lines mark the temperature limits imposed by resolution (grey) and SNR (red), respectively. The $\text{SNR} \leq 1$ regime assumes a destruction limit of $D = 0.01$. The area below both limits (filled, blue) is where thermal density fluctuations are resolvable by the measurement. Temperature is in units of Fermi temperature $k_B T_F = \hbar \omega_{\perp} (6N\kappa)^{1/3}$ and critical condensation temperature $k_B T_c^0 \approx \hbar(\kappa)^{1/3} \omega_{\perp} N^{1/3}$ for (a) and (b), respectively.

$R_i \approx \sqrt{\hbar/(m\omega_i)} (48N\kappa)^{1/6}$ [41] and $R_i = \sqrt{\hbar/(m\omega_i)}$, respectively. Equation (2) then implies

$$D \geq \frac{16\pi^2 \hbar^2}{A \sigma_0 m^2 \omega_{\perp}^2} \begin{cases} N^{-2}, & \text{bosons,} \\ (48\kappa)^{2/3} N^{-4/3}, & \text{fermions.} \end{cases} \quad (3)$$

This demonstrates that achieving the required SNR for degenerate Fermi gases requires a factor of $(48N\kappa)^{2/3}$ more destruction than for similar bosonic species, due to degeneracy pressure.

Finally, we require a measurement resolution no larger than the thermal de Broglie wavelength $\lambda_{\text{DB}}(T) = \sqrt{2\pi\hbar^2/(mk_B T)}$: $\Delta r \leq \lambda_{\text{DB}}(T)$ and $A \leq \lambda_{\text{DB}}(T)^2$. Combining this with Eq. (1) and Eq. (3) gives the parameter regime where feedback cooling is effective (in the absence of rethermalization). To apply Eq. (2), we must choose an acceptable amount of destruction per measurement – here we take this to be an absorption of 1% per measurement, fixing $D = 0.01$. For a concrete comparison, we consider ${}^6\text{Li}$ and ${}^7\text{Li}$ as exemplary fermionic and bosonic species, as they have similar mass and electronic D1 ($\lambda = 670\text{nm}$) transition [42].

Figure 2 plots the regions bounded by our inequalities for trapping parameters $\{\omega_{\perp}/2\pi, \kappa\} = \{10 \text{ Hz}, 10^2\}$, and compares the degenerate Fermi and ideal Bose cases. This shows that the regime of (T, N) values where excitations are resolvable is much narrower for degenerate Fermi gases than degenerate ideal Bose gases. Since this narrow regime is beyond the capability of modern Fermi gas experiments, both in achievable atom number and temperature [26], this rules out the use of feedback cooling for single-component Fermi gases in the degenerate regime. In contrast, excitations are resolvable across the degenerate regime for Bose gases – although, as shown below, this is not required for effective cooling due to rethermalization via interparticle scattering.

Thermodynamic model of feedback cooling.— Here we develop a thermodynamic model of feedback cooling, based on the underlying premise that you can ‘only control what you can see’. That is, the fraction of total energy removable depends on the excitations resolvable with the spatial resolution of the imaging. We divide the atomic cloud into 2D cells of area A , corresponding to the pixel size of the spatially-filtered atomic density image. Each cell contains N_A particles each contributing $3k_B T$ of energy [43], giving a total energy $E = 3N_A k_B T$ per cell. Optical imaging only measures the cell’s center-of-mass (COM) motion in the xy plane, which by equipartition contains $2k_B T$ of energy. Thus, without rethermalization, feedback can at best extract a fraction of the total energy $\delta \equiv \Delta E/E \leq 2/(3N_A)$. Here ΔE is the energy removed by the feedback; $\delta = 1$ corresponds to removal of all energy from the cloud. However, in general, the resolution limit Eq. (1) implies that N_A cannot be reduced to the single-particle detection regime needed to extract the majority of the cloud’s energy.

The achievable δ is reduced by the finite measurement SNR, which gives a misestimation of the atom number in each pixel, $\Delta N_A = N_A/\text{SNR}$. This prevents the perfect extraction of COM energy via feedback, giving residual COM energy $2(\Delta N_A/N_A)k_B T$ and thus a more realistic bound on the fraction of energy removable by feedback: $\delta \leq 2(1 - \text{SNR}^{-1})/(3N_A)$. In principle, we can maximize δ by optimizing the pixel size A for a given column density \bar{n} , however, for sufficiently large \bar{n} it is generally optimal to choose $A = r_D^2$ (the fundamental resolution limit) and instead optimize D to minimize heating.

There are two channels of measurement-induced heating that further reduce the achievable δ . Firstly, each spontaneous emission event heats the atomic cloud by twice the photon recoil energy, assuming a sufficiently deep trap such that the recoil does not induce loss. This contributes energy $2N_A D p_{\text{re}}^2/m$ to each pixel per image, where $p_{\text{re}} = \hbar k$ is the photon recoil momentum. Secondly, the fundamental measurement backaction heats the sample, with the atom-light interaction causing phase gradients in the atomic wavefunction that contribute kinetic energy (see Eq. (A13) in Appendix A for an estimate of the backaction heating magnitude). Together, these two heating channels increase the fraction of energy per pixel by $D\epsilon/(k_B T)$ with each measurement, where the energy-scale $\epsilon \equiv 4p_{\text{re}}^2/(6m) + \pi\hbar^2/(2mR_z^2)$ includes the respective contributions from spontaneous emission and backaction.

Incorporating both measurement-induced heating contributions into the bound set by finite measurement SNR, we find that for \mathcal{M} images taken per cycle of feedback, the best achievable net fraction of energy removed is:

$$\delta = \frac{2}{3\bar{n}r_D^2} (1 - \text{SNR}^{-1}) - \mathcal{M}D \frac{\epsilon}{k_B T}, \quad (4)$$

where we have maximum imaging resolution ($A = r_D^2$)

by the substitution $N_A = \bar{n}A$. Recall that the upper bound on the SNR is proportional to \sqrt{D} ; thus heating cannot be reduced arbitrarily by reducing D . Since $R_z^2 \gg \lambda^2$ in the thermal gas regime, spontaneous emission heating dominates over backaction (Appendix A), giving $\epsilon \approx 4k_B T_{\text{re}}/3$, where $T_{\text{re}} = p_{\text{re}}^2/(2mk_B)$ is the recoil temperature.

Since cooling is only possible for $\delta \geq 0$, Eq. (4) lets us determine the minimum temperature achievable by feedback cooling (see Appendix B):

$$T \geq T_{\text{min}} \equiv \frac{3\mathcal{M}}{2\eta\bar{n}\sigma_0} \frac{\epsilon}{k_B} \approx \frac{2\mathcal{M}}{\eta\bar{n}\sigma_0} T_{\text{re}}. \quad (5)$$

This bound naïvely suggests the temperature can be made arbitrarily small by making the column density \bar{n} arbitrarily large, and increasing the detuning accordingly to ensure the sample remains in the optically thin regime $\bar{n}\sigma_0 \ll 1 + 4\Delta^2/\Gamma^2$. However, \bar{n} is limited by the peak 3D atom density via $n_{3D} = \bar{n}_{\text{max}}/(\sqrt{2\pi}R_z)$, which cannot exceed a critical value n_{crit} set by three-body recombination losses [44]. As an example, consider a ^{87}Rb cloud with $n_{\text{crit}} \sim 10^{14}\text{cm}^{-3}$; for $R_z \approx 1\mu\text{m}$, Eq. (5) gives $T_{\text{min}} \approx 5\text{nK}$. This is well below typical transition temperatures ($\sim 1\mu\text{K}$), suggesting feedback is capable of cooling thermal Bose gases to degeneracy.

Continuous cooling with rethermalization.— Following feedback, the atomic cloud will rethermalize to a slightly lower temperature (provided $\delta > 0$) $T_{\text{new}} = T_{\text{old}}(1 - \delta)$ [45] on a timescale set by the elastic collision rate $\Delta t^{-1} \equiv \gamma_{\text{el}} = n_{3D}\sigma_s\sqrt{2}v_{\text{th}}$, where σ_s is the s-wave scattering cross-section and $v_{\text{th}} = \sqrt{8k_B T/(\pi m)}$ is the thermal atomic velocity. For large atomic densities, each stage of feedback can only reduce the energy by a small fraction $\delta \ll 1$. Therefore, for fast rethermalization we can take the infinitesimal limit of $(T_{\text{new}} - T_{\text{old}})/\Delta t$ to obtain:

$$\frac{dT}{dt} = -\gamma_{\text{el}}(T)\delta(T)T, \quad (6)$$

where δ depends on T through the implicit temperature dependence of the atomic density.

We can bound the cooling rate $\gamma \equiv |dT/dt|/T$ using Eq. (6) and $\delta \leq 2/(3\bar{n}r_D^2)$:

$$\gamma \leq \frac{4\pi}{3} \frac{\gamma_{\text{el}}(T)\sigma_s}{\bar{n}\lambda R_z} \approx \frac{4\sqrt{\pi}}{3} \frac{v_{\text{th}}(T)\sigma_s}{\lambda R_z^2}. \quad (7)$$

This expression is independent of atom number; while increasing the atom density via increasing N speeds up rethermalization, it also reduces the fraction of energy stored in the COM motional energy of each pixel by the same amount (for fixed A). Equation (7) also demonstrates the importance of tight trapping in the imaging direction. Since we require $R_{\perp} \gg r_D$ for high-resolution spatial imaging, this suggests feedback cooling will be

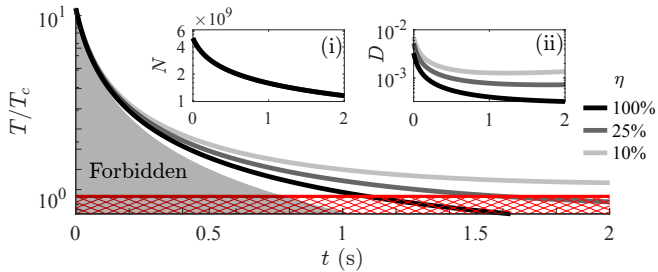


FIG. 3. Feedback cooling an oblate ^{87}Rb cloud of fixed spatial size $\{R_{\perp}, \kappa\} \approx \{522\mu\text{m}, 150\}$ with initial number $N(0) = 5 \times 10^9$ and temperature $T(0) = 180\mu\text{K}$, for varied detection efficiencies η . Feedback can only extract energy visible in the finite-resolution imaging; violation of $\delta < 2/(3N_A)$ defines a forbidden region (grey, shaded). (i) Roughly 80% of the initial sample is lost over 2s due to three-body recombination. (ii) Measurement destruction is optimized at each timestep to minimize heating. Calculations assume a thermal gas; below T_c (red, hatched) the model breaks down.

most effective for highly oblate gases, i.e. $\kappa \gg 1$ geometries. For the above ^{87}Rb example, $T = 100\mu\text{K}$ ($10\mu\text{K}$) gives $\gamma \lesssim 35\text{Hz}$ (110Hz).

Exemplary cooling demonstration.— We have shown that feedback cooling is most effective when the atomic density is as large as three-body recombination permits, since this gives high SNR and fast rethermalization. One method of maintaining high density during cooling is to reduce the trapping frequency as $\omega(t) = \omega(0)\sqrt{T(t)/T(0)}$; this keeps R_{\perp}, R_z , and thus the atomic density, constant. In Fig. 3 we use Eq. (6) to model such an experiment, where a large ^{87}Rb cloud with initial atom number $N(0) = 5 \times 10^9$ and temperature $T = 180\mu\text{K}$ (typical parameters after Doppler cooling) is held in a trap with $\omega_{\perp}(0)/2\pi = 40\text{Hz}$ and fixed aspect ratio $\kappa = 150$. The measurement strength (parameterized by destruction D) is chosen at each time step to optimize the trade-off between SNR and measurement-induced heating (see Eq. (B1) in Appendix B). For these parameters, feedback cools the cloud to the critical temperature $T_c \sim 1\mu\text{K}$ in 1–2 seconds, while the atom number only reduces by 5× to $N \sim 10^9$ – a performance impossible to achieve in alkali atoms with traditional cooling techniques (laser cooling, followed by evaporation).

Our feedback cooling protocol is robust to imperfect detector efficiency (or equivalently, technical imaging noise), with similar cooling achievable with $\eta = 25\%$ (compared to perfect detection). For lower values of η , Fig. 3 shows the temperature plateauing at micro-Kelvin temperatures just above T_c due to the SNR approaching unity; cooling further would require an increase in density that would lead to further atom loss.

Discussion.— In principle, feedback could cool atomic gases to degeneracy from arbitrarily high temperatures with minimal atom loss – in fact, for higher temperatures the measurement heating becomes negligible and

the rethermalization rate increases. In practice, cooling performance will be limited by time delay in the feedback loop, which will preclude cooling of density fluctuations on shorter timescales. We can estimate the timescale of these fluctuations by the average time taken for atoms to move across pixels, i.e. $\tau \equiv 2\Delta r/v_{\text{th}}(T)$. For ^{87}Rb imaged at the resolution limit $\Delta r = r_D$ for $T = 10\mu\text{K}$ ($200\mu\text{K}$), $\tau \approx 20\mu\text{s}$ ($5\mu\text{s}$). Note that it is the time delay between measurement and feedback that must be shorter than τ ; in principle, the period between applications of feedback can be longer than τ , enabling the use of modern spatial light modulators with switching speeds of 20kHz [22]. The impact of time delay can be partially mitigated by feeding back on broader density fluctuations (i.e. setting $\Delta r > r_D$), at the cost of slowing down cooling by a factor of $(\Delta r/r_D)^2$.

Our model of continuous feedback cooling can be straightforwardly extended to describe the sympathetic cooling of multi-component atomic clouds via interaction with a feedback-cooled source. That is, the measurement and feedback cooling of a single component allows the extraction of energy from other components due to interatomic scattering between components and rethermalization. This could, for example, describe the feedback cooling of Bose-Fermi or Fermi-Fermi mixtures. For an M component system of equal local density, each pixel contains $3MN_A$ degrees of freedom, yet only two COM degrees of freedom can be controlled. Following our earlier argument, we thus find the fraction of energy observable from optical imaging is a factor M smaller than the single-component case (i.e. $\delta_{\text{multi}} \leq 2/(3MN_A)$). Furthermore, σ_s is reduced by 1/2 for intercomponent scattering as compared to scattering of identical particles, which makes the cooling rate in the sympathetic-cooling case $2M \times$ slower than if each component were measured and feedback-cooled individually (c.f. Eq. (7)).

Our feedback model is constructed in the thermal gas regime; it breaks down qualitatively in the degenerate regime since quantum statistics affect rethermalization. For Bose gases, we expect feedback cooling to dramatically improve near degeneracy, since the specific heat capacity sharply drops and there is Bose-enhanced transfer into the condensate mode. Precisely the opposite will happen for purely fermionic mixtures, as Pauli blocking significantly reduces the elastic scattering rate [46, 47]. However, feedback could still prove advantageous in this regime by allowing much larger atom numbers than is accessible from evaporation. Furthermore, we expect feedback could enhance sympathetic cooling of Fermi-Bose mixtures, which in the evaporative case is limited by the vanishing heat capacity of the Bose component [26]; extracting energy from the Bose gas via feedback could ameliorate this limitation and provide a pathway to achieving deeper Fermi degeneracy with large N .

In the degenerate regime, there are models of the partially coherent atomic dynamics which may allow real-

time state estimation and filtering [30, 32, 48]. This could enable more sophisticated control than permitted by our model, which may allow effective feedback with weaker measurement or better control with the same measurement SNR. Nevertheless, implementing a real-time filter of the full-field dynamics is a highly-challenging prospect; we expect near-term demonstrations will instead use simple spatiotemporal filters to improve the SNR of the real-time density estimates.

Conclusions.— We have shown that feedback cooling could produce large atom-number quantum gases in low-dimensional geometries, beyond the fundamental capability of traditional evaporative cooling techniques. As our analysis is based on generic thermodynamic arguments and key operating principles of non-destructive optical measurement, these results are applicable to a broad range of experimental scenarios. Our work confirms that near-term proof-of-principle demonstrations are certainly within the capability of established cold-atom experiments.

APPENDICES

A. Quantum backaction heating

Here we estimate the heating effect due to fundamental quantum backaction. Our analysis is simplified by dividing the atomic density measurement into number measurements on spatial cells of area r_D^2 , where r_D is the fundamental resolution of the dispersive imaging, and treating each cell as being subjected to a quantum non-demolition (QND) number measurement. Measurement backaction scrambles the relative phase between cells, with a strength dependent on the number measurement precision. As a baseline, we expect the phase relation between unmeasured cells to be given by the magnitude of relative number fluctuations, $1/\sqrt{N_{\text{cell}}}$.

The QND measurement of a single cell is described by the unitary:

$$\hat{U}_{\text{QND}} = \exp\left(i\beta\hat{N}_p\hat{N}_{\text{cell}}\right), \quad (\text{A1})$$

where \hat{N}_p is the photon number operator and β is a constant of proportionality we will relate to the shot-noise-limited SNR. Firstly, this unitary applies a phase to the light field $\phi_{\text{light}} = \beta N_{\text{cell}}$, with fluctuations given by the shot-noise relation

$$\Delta\phi_{\text{light}} = \frac{1}{\sqrt{N_p}} = \beta\Delta N_{\text{cell}}. \quad (\text{A2})$$

Secondly, the QND unitary applies a phase $\phi_{\text{atom}} = \beta N_p$ to the atomic state, with associated fluctuation $\Delta\phi_{\text{atom}} = \beta\sqrt{N_p}$. Combining this with Eq. (A2) relates the magnitude of measurement-induced atomic phase fluctuations

to the precision with which N_{cell} can be estimated:

$$\Delta\phi_{\text{atom}} = \frac{1}{\Delta N_{\text{cell}}} = \frac{\text{SNR}_{\text{cell}}}{N_{\text{cell}}}, \quad (\text{A3})$$

where SNR_{cell} is the fundamental limit to the measurement sensitivity, given by the RHS of Eq. (2) with $A = r_D^2$ and $\eta = 1$. This expression demonstrates that stronger measurement gives larger phase fluctuations, and hence stronger backaction. For example, a perfect (projective) number measurement will give $\Delta N = 0$ and hence infinitely strong phase fluctuations.

To relate this to heating, we assume these phase fluctuations give rise to phase gradients $\partial_x\phi(x) \approx \Delta\phi_{\text{atom}}/r_D$. This translates to a kinetic energy contribution, which we can compute by treating the gas as locally homogeneous over each cell. For a single cell this gives an energy contribution:

$$E_{\text{BA}}^{\text{cell}} = -\frac{\hbar^2}{2m} \left\langle \int_{\text{cell}} dx dy \hat{\psi}^\dagger(\mathbf{x}) \nabla^2 \hat{\psi}(\mathbf{x}) \right\rangle \quad (\text{A4})$$

$$\approx \frac{\hbar^2}{2m} N_{\text{cell}} \int_{\text{cell}} \frac{dx dy}{r_D^2} |\nabla \phi(\mathbf{x})|^2 \quad (\text{A5})$$

$$\approx \frac{\hbar^2}{m} N_{\text{cell}} \left(\frac{\Delta\phi_{\text{atom}}}{r_D} \right)^2, \quad (\text{A6})$$

where $\hat{\psi}(\mathbf{x})$ is the atomic field operator in the plane transverse to the imaging axis. The total energy added to each pixel is given by multiplying $E_{\text{BA}}^{\text{cell}}$ by the number of cells on each pixel A/r_D^2 . Substituting in $N_{\text{cell}} = N_A r_D^2/A$, $\Delta\phi_{\text{atom}} = \text{SNR}/N_{\text{cell}}$, and $\text{SNR}_{\text{cell}} = (\bar{n}/2)\sqrt{r_D^2\sigma_0 D}$, we can express this energy as:

$$E_{\text{BA}} = \frac{A}{r_D^2} \frac{\hbar^2}{m} N_{\text{cell}} \left(\frac{\text{SNR}_{\text{cell}}}{N_{\text{cell}} r_D} \right)^2 \quad (\text{A7})$$

$$= \frac{A}{r_D^2} \frac{\hbar^2}{m} \frac{N_A r_D^2}{A} \left(\frac{\text{SNR}_{\text{cell}}}{N_{\text{cell}} r_D} \right)^2 \quad (\text{A8})$$

$$= N_A \frac{\hbar^2 \bar{n}^2 \sigma_0 r_D^2 D}{m} \frac{A^2}{4r_D^2} \frac{1}{N_A^2 r_D^4} \quad (\text{A9})$$

$$= N_A D \frac{\hbar^2}{2m} \frac{\sigma}{2r_D^4} \quad (\text{A10})$$

where in the last line we have used $\bar{n} = N_A/A$. This takes the form of a free-particle dispersion relation with wavevector $\sqrt{\sigma_0/r_D^4}$. Substituting the cross-sectional area of the light $\sigma_0 = 3\lambda^2/2\pi$ and resolution limit $r_D = \sqrt{R_z\lambda/(2\pi)}$, we see that the above relation depends only on the gas thickness:

$$E_{\text{BA}} = N_A D \frac{\hbar^2}{4m} \frac{3\lambda^2}{2\pi} \frac{(2\pi)^2}{(R_z\lambda)^2} \quad (\text{A11})$$

$$= 3N_A \frac{\hbar^2}{2m} \frac{D\pi}{R_z^2} \quad (\text{A12})$$

from which we obtain a heating contribution to δ of

$$\delta_{\text{BA}} = -\frac{\hbar^2}{2m R_z^2} \frac{\pi D}{k_B T}. \quad (\text{A13})$$

We can compare this to the heating contribution from spontaneous emission δ_{SE} ,

$$\frac{\delta_{\text{BA}}}{\delta_{\text{SE}}} = \frac{3\pi}{64} \left(\frac{\lambda}{R_z} \right)^2, \quad (\text{A14})$$

showing that spontaneous emission heating dominates over backaction heating if $R_z^2 \gg \lambda^2$.

B. Derivation of temperature bound

Starting with Eq. (4), we can analytically optimize the choice of D . Assuming the SNR saturates the bound Eq. (2) with a resolution at the fundamental limit $A = r_D^2$, the choice of D that maximizes δ is:

$$D_{\text{opt}} = \left(\frac{4k_B^2 T^2}{9\bar{n}^4 r_D^6 \epsilon^2 \eta \sigma_0} \right)^{1/3}, \quad (\text{B1})$$

In practice, the temperature T can be estimated from the observable standard deviation of the atomic cloud R_{\perp} .

We can then derive the temperature bound Eq. (5) by substituting Eq. (B1) into Eq. (4) and solving for $\delta \geq 0$, which is the region where the increase in energy due to measurement-induced heating is greater than the amount of energy feedback can extract:

$$\delta_{\text{opt}} = \frac{2}{3\bar{n}r_D^2} \left(1 - \frac{2}{\bar{n}\sqrt{\eta A \sigma_0 D_{\text{opt}}}} \right) - \mathcal{M} D_{\text{opt}} \frac{\epsilon}{k_B T} \geq 0.$$

Solving the above inequality directly for T does not lead to an insightful expression for the bound on the temperature. We may obtain a simple analytic expression by further assuming the column density \bar{n} is sufficiently large that the shot-noise-limited SNR is significantly greater than unity, allowing the second bracketed term to be neglected. Then, solving the above equation for T yields Eq. (5) of the main text.

C. Details of numerical simulation

Here we outline the details of the numerical simulation used to produce Fig. 3. The simulation is based on the continuous model Eq. (6) where the fraction of energy extracted per shot of feedback $\delta(T)$ is computed at each timestep using Eq. (4) with $\mathcal{M} = 1$. These calculations use parameters corresponding to ^{87}Rb (s-wave scattering length $a_s = 100.4a_0$, where a_0 is the Bohr radius), with the optical imaging far-detuned from the D_2 transition ($\lambda = 780\text{nm}$).

Our calculations also incorporate atom loss due to three-body recombination. We start with the rate equation describing three-body loss [44]:

$$\frac{dn_{3d}}{dt} = -K n_{3d}^3, \quad (\text{C1})$$

where K is the three-body loss rate that is empirically determined. For ^{87}Rb , $K \approx 4 \times 10^{-41}\text{m}^6/\text{s}$ [49] – this sets the density scale at which loss becomes significant, $\mathcal{O}(10^{14})\text{cm}^{-3}$. We recast this equation in terms of the atom number N using the Gaussian description of the atomic density employed in the main text,

$$\frac{dN}{dt} = -KN(t) \left(\frac{N(t)}{(2\pi)^{3/2} R_{\perp}^2 R_z} \right)^2. \quad (\text{C2})$$

We solve the coupled differential equations (6) and (C2) with a fourth-order Runge-Kutta algorithm (adaptive timestep). At each timestep, $\delta(T)$ is computed using Eq. (4) with $\mathcal{M} = 1$ and $\bar{n} = N/(2\pi R_{\perp}^2)$.

- [1] C. E. Wieman, D. E. Pritchard, and D. J. Wineland, Rev. Mod. Phys. **71**, S253 (1999).
- [2] D. Leibfried, R. Blatt, C. Monroe, and D. Wineland, Rev. Mod. Phys. **75**, 281 (2003).
- [3] M. Aspelmeyer, T. J. Kippenberg, and F. Marquardt, Rev. Mod. Phys. **86**, 1391 (2014).
- [4] F. Fröwis, P. Sekatski, W. Dür, N. Gisin, and N. Sangouard, Rev. Mod. Phys. **90**, 025004 (2018).
- [5] C. L. Degen, F. Reinhard, and P. Cappellaro, Rev. Mod. Phys. **89**, 035002 (2017).
- [6] I. Bloch, J. Dalibard, and W. Zwerger, Rev. Mod. Phys. **80**, 885 (2008).
- [7] C. W. Bauer, Z. Davoudi, A. B. Balantekin, T. Bhattacharya, M. Carena, W. A. de Jong, P. Draper, A. El-Khadra, N. Gemelke, M. Hanada, D. Kharzeev, H. Lamm, Y.-Y. Li, J. Liu, M. Lukin, Y. Meurice, C. Monroe, B. Nachman, G. Pagano, J. Preskill, E. Rinaldi, A. Roggero, D. I. Santiago, M. J. Savage, I. Siddiqi, G. Siopsis, D. Van Zanten, N. Wiebe, Y. Yamauchi, K. Yeter-Aydeniz, and S. Zorzetti, PRX Quantum **4**, 027001 (2023).
- [8] M. Saffman, T. G. Walker, and K. Mølmer, Rev. Mod. Phys. **82**, 2313 (2010).
- [9] B. J. Brown, D. Loss, J. K. Pachos, C. N. Self, and J. R. Wootton, Rev. Mod. Phys. **88**, 045005 (2016).
- [10] J. Zhang, Y. xi Liu, R.-B. Wu, K. Jacobs, and F. Nori, Physics Reports **679**, 1 (2017).
- [11] P. Bushev, D. Rotter, A. Wilson, F. m. c. Dubin, C. Becher, J. Eschner, R. Blatt, V. Steixner, P. Rabl, and P. Zoller, Phys. Rev. Lett. **96**, 043003 (2006).
- [12] P. F. Cohadon, A. Heidmann, and M. Pinard, Phys. Rev. Lett. **83**, 3174 (1999).
- [13] J. Guo, R. Norte, and S. Gröblacher, Phys. Rev. Lett. **123**, 223602 (2019).
- [14] M. Rossi, D. Mason, J. Chen, Y. Tsaturyan, and A. Schliesser, Nature **563**, 53 (2018).
- [15] D. J. Wilson, V. Sudhir, N. Piro, R. Schilling, A. Ghadimi, and T. J. Kippenberg, Nature **524**, 325 (2015).
- [16] T. Li, S. Kheifets, and M. G. Raizen, Nature Physics **7**, 527 (2011).
- [17] M. Poggio, C. L. Degen, H. J. Mamin, and D. Rugar, Phys. Rev. Lett. **99**, 017201 (2007).
- [18] L. Magrini, P. Rosenzweig, C. Bach, A. Deutschmann-

Olek, S. G. Hofer, S. Hong, N. Kiesel, A. Kugi, and M. Aspelmeyer, *Nature* **595**, 373 (2021).

[19] F. Tebbenjohanns, M. L. Mattana, M. Rossi, M. Frimmer, and L. Novotny, *Nature* **595**, 378 (2021).

[20] J. Vovrosh, M. Rashid, D. Hempston, J. Bateman, M. Paternostro, and H. Ulbricht, *Journal of the Optical Society of America B* **34**, 1421 (2017).

[21] K. Henderson, C. Ryu, C. MacCormick, and M. G. Boshier, *New Journal of Physics* **11**, 043030 (2009).

[22] G. Gauthier, I. Lenton, N. M. Parry, M. Baker, M. J. Davis, H. Rubinsztein-Dunlop, and T. W. Neely, *Optica* **3**, 1136 (2016).

[23] G. Gauthier, T. A. Bell, A. B. Stilgoe, M. Baker, H. Rubinsztein-Dunlop, and T. W. Neely, in *Advances In Atomic, Molecular, and Optical Physics* (Elsevier, 2021) pp. 1–101.

[24] P. B. Wigley, P. J. Everitt, A. van den Hengel, J. W. Bastian, M. A. Sooriyabandara, G. D. McDonald, K. S. Hardman, C. D. Quinlivan, P. Manju, C. C. N. Kuhn, I. R. Petersen, A. N. Luiten, J. J. Hope, N. P. Robins, and M. R. Hush, *Sci. Rep.* **6** (2016).

[25] A. Belenchia, M. Carlesso, Ömer Bayraktar, D. Dequal, I. Derkach, G. Gasbarri, W. Herr, Y. L. Li, M. Rademacher, J. Sidhu, D. K. Oi, S. T. Seidel, R. Kaltenbaek, C. Marquardt, H. Ulbricht, V. C. Usenko, L. Wörner, A. Xuereb, M. Paternostro, and A. Bassi, *Physics Reports* **951**, 1 (2022).

[26] R. Onofrio, *Physics-Uspekhi* **59**, 1129 (2016), publisher: IOP Publishing.

[27] S. A. Haine, A. J. Ferris, J. D. Close, and J. J. Hope, *Phys. Rev. A* **69**, 013605 (2004).

[28] S. D. Wilson, A. R. R. Carvalho, J. J. Hope, and M. R. James, *Physical Review A* **76**, 013610 (2007), publisher: American Physical Society.

[29] S. S. Szigeti, M. R. Hush, A. R. R. Carvalho, and J. J. Hope, *Phys. Rev. A* **80**, 013614 (2009).

[30] S. S. Szigeti, M. R. Hush, A. R. R. Carvalho, and J. J. Hope, *Phys. Rev. A* **82**, 043632 (2010).

[31] S. S. Szigeti, *Physical Review A* **87** (2013), 10.1103/PhysRevA.87.013626.

[32] M. R. Hush, S. S. Szigeti, A. R. R. Carvalho, and J. J. Hope, *New J. Phys* **15**, 113060 (2013).

[33] H. M. Hurst, S. Guo, and I. B. Spielman, *Phys. Rev. Research* **2**, 043325 (2020).

[34] A. C. Wade, J. F. Sherson, and K. Mølmer, *Physical Review Letters* **115**, 060401 (2015), publisher: American Physical Society.

[35] A. C. J. Wade, J. F. Sherson, and K. Mølmer, *Physical Review A* **93**, 023610 (2016), publisher: American Physical Society.

[36] M. Schemmer, A. Johnson, R. Photopoulos, and I. Bouchoule, *Phys. Rev. A* **95**, 043641 (2017).

[37] M. L. Goh, Z. Mehdi, R. L. Taylor, R. J. Thomas, A. S. Bradley, M. R. Hush, J. J. Hope, and S. S. Szigeti, “Feedback cooling bose gases to quantum degeneracy,” (2022).

[38] D. A. R. Dalvit, J. Dziarmaga, and R. Onofrio, *Phys. Rev. A* **65**, 053604 (2002).

[39] J. J. Hope and J. D. Close, *Physical Review Letters* **93** (2004), 10.1103/physrevlett.93.180402.

[40] J. J. Hope and J. D. Close, *Physical Review A* **71**, 043822 (2005), publisher: American Physical Society.

[41] S. Giorgini, L. P. Pitaevskii, and S. Stringari, *Reviews of Modern Physics* **80**, 1215 (2008).

[42] Other commonly used atomic species have key parameters (mass and electronic transition wavelength) on the same order of magnitude.

[43] We neglect low-temperature corrections to the heat capacity of harmonically-trapped bosons, which are only significant near the critical condensation temperature $T \lesssim 2T_c$ [50].

[44] C. J. Pethick and H. Smith, *Bose-Einstein Condensation in Dilute Gases* (Cambridge University Press, 2008).

[45] This neglects the slight temperature dependence of the heat capacity near T_c .)

[46] M. J. Holland, B. DeMarco, and D. S. Jin, *Phys. Rev. A* **61**, 053610 (2000).

[47] M. Crescimanno, C. G. Kaoy, and R. Peterson, *Phys. Rev. A* **61**, 053602 (2000).

[48] D. Dong and I. R. Petersen, *Annual Reviews in Control* **54**, 243 (2022).

[49] P. J. Everitt, M. A. Sooriyabandara, M. Guasoni, P. B. Wigley, C. H. Wei, G. D. McDonald, K. S. Hardman, P. Manju, J. D. Close, C. C. N. Kuhn, S. S. Szigeti, Y. S. Kivshar, and N. P. Robins, *Phys. Rev. A* **96**, 041601 (2017).

[50] S. Biswas and D. Jana, *European Journal of Physics* **33**, 1527 (2012)